Biosensors and Bioelectronics 77 (2016) 580–588

Contents lists available at ScienceDirect

Biosensors and Bioelectronics

journal homepage: www.elsevier.com/locate/bios

Gold-coated carbon nanotube electrode arrays: Immunosensors for impedimetric detection of bone biomarkers

Madhumati Ramanathan [a,1], Mitali Patil [a,1], Rigved Epur [b], Yeoheung Yun [c], Vasselin Shanov [d], Mark Schulz [e], William R. Heineman [f], Moni K. Datta [a], Prashant N. Kumta [a,b,g,h,*]

[a] Department of Bioengineering, Swanson School of Engineering, University of Pittsburgh, Pittsburgh, PA, United States
[b] Department of Mechanical Engineering and Materials Science, Swanson School of Engineering, University of Pittsburgh, Pittsburgh, PA, United States
[c] Chemical and Bioengineering Department, North Carolina A&T State University, Greensboro, NC, United States
[d] Department of Mechanical Engineering, University of Cincinnati, Cincinnati, OH, United States
[e] Department of Chemical and Materials Engineering, University of Cincinnati, Cincinnati, OH, United States
[f] Department of Chemistry, University of Cincinnati, Cincinnati, OH, United States
[g] Department of Chemical and Petroleum Engineering, Swanson School of Engineering, University of Pittsburgh, Pittsburgh, PA, United States
[h] Department of Oral Biology, School of Dental Medicine, University of Pittsburgh, Pittsburgh, PA, United States

ARTICLE INFO

Article history:
Received 22 June 2015
Received in revised form
16 September 2015
Accepted 5 October 2015
Available online 14 November 2015

Keywords:
CNT
Gold nanoparticles
Immunosensor
Impedance
C-terminal telopeptide
Bone marker

ABSTRACT

C-terminal telopeptide (cTx), a fragment generated during collagen degradation, is a key biomarker of bone resorption during the bone remodeling process. The presence of varying levels of cTx in the bloodstream can hence be indicative of abnormal bone metabolism. This study focuses on the development of an immunosensor utilizing carbon nanotube (CNT) electrodes coated with gold nanoparticles for the detection of cTx, which could ultimately lead to the development of an inexpensive and rapid point-of-care (POC) tool for bone metabolism detection and prognostics. Electrochemical impedance spectroscopy (EIS) was implemented to monitor and detect the antigen–antibody binding events occurring on the surface of the gold-deposited CNT electrode. Type I cTx was used as the model protein to test the developed sensor. The sensor was accordingly characterized at various stages of development for evaluation of the optimal sensor performance. The biosensor could detect cTx levels as low as 0.05 ng/mL. The feasibility of the sensor for point-of-care (POC) applications was further demonstrated by determining the single frequency showing maximum changes in impedance, which was determined to be 18.75 Hz.

1. Introduction

Millions of individuals suffer from various forms of musculoskeletal disorders such as bone carcinoma or osteoporosis as a result of poor bone health. When these bone diseases are not treated efficiently in a timely fashion, bone health can deteriorate leading to further complications and possible fatality. 44 million Americans currently suffer from low bone density or osteoporosis, and 24% of hip fracture patients older than age 50 suffer fatalities a year after injury (Burge et al., 2007). The annual cost arising from musculoskeletal disorders alone in the United States is approximately $850 billion and the costs associated with osteoporosis related fractures exclusively are projected to reach $25 billion by 2025 (National Osteoporosis Foundation, 2012). Hence, in light of the increasing trend in the geriatric population and the escalating costs of healthcare, it is critical to detect and monitor any changes in bone modeling and remodeling for effective treatment of bone diseases during the developmental stage and preserving ambulatory functions.

Bone health is characterized by the adaptation of bone to external loading through modeling and remodeling metabolic processes via various cellular mechanisms. These processes influence the bone's mechanical structural integrity and strength by modifying the size, shape, and the micro- and macro-architecture of bone (Seeman and Delmas, 2006; Ryouji et al., 2000). During bone metabolism, bone turnover markers are released into the bloodstream and in the urine, thus serving as an indicative marker of the bone modeling and remodeling process. Therefore, changes in the bone metabolism during the bone resorption and bone formation process will be reflected in the bone turnover marker

* Correspondence to: Department of Bioengineering, Chemical and Petroleum Engineering, Mechanical Engineering and Materials Science, University of Pittsburgh, 815C Benedum Hall, 3700 O'Hara Street, Pittsburgh, PA 15261, United States.
E-mail address: pkumta@pitt.edu (P.N. Kumta).
[1] Contributed equally.

http://dx.doi.org/10.1016/j.bios.2015.10.014
0956-5663/

levels. Bone turnover markers can be particularly useful in understanding bone physiology, assessing facture risks (particularly wherein bone resorption occurs faster than bone formation), and more importantly, determining the response of bone to treatment (Burgeson, 1998; Okuno et al., 2005; Rosenquist et al., 1998).

During the remodeling process of bone, type I collagen is degraded and small peptide fragments are secreted into the blood stream and urine, including the bone resorption marker C-terminal telopeptide (cTx) (Srivastava et al., 2001). Bone turnover markers such as cTx are being studied as clinical research tools, but are not measured frequently in the same patient due to the variation in the levels from day to day or even across a given day. Moreover, the current method of detection of bone turnover markers is based upon enzyme-linked immunosorbent assay (ELISA) which is time consuming, expensive, and more importantly, involves several steps for incubation, antibody binding, and fluorescence measurement (Ross, 1999; Srivastava et al., 2001). Therefore, it would be more useful and beneficial to develop an electrochemical POC biosensor that can quantitatively determine the bone turnover markers in a timely and inexpensive fashion. This development can be achieved by exploiting electrochemical impedance spectroscopy (EIS) for the detection of bone turnover makers. EIS is a label-free operation that does not require secondary labeling, and the impedance based technique is extremely sensitive to interfacial binding events occurring at the probe surface. This is especially critical when developing sensitive detection platforms that are immune to bulk processes occurring in the sample matrix, thus making an impedimetric electronic biosensor particularly advantageous (Daniels and Pourmand, 2007; Katz and Willner, 2003).

Carbon nanotubes (CNTs) have gained considerable attention amongst the various materials used in the development of biosensors due to their exceptional mechanical, electrical and surface properties (Ahammad et al., 2009; Ajayan, 1999; Saito et al., 2009; Tasis et al., 2006). The facile bottom–up approach to grow them is particularly well suited as the growth conditions may be modified to achieve specific properties to fit and meet the needs for sensor integration (Chakrabarti et al., 2007; Landis et al., 2010; Yun et al., 2006). Studies have also been performed to understand the influence of the nanotube side walls, tips and their size, on their electron transfer kinetics (Gong et. al., 2008; Siddiqui et al., 2010). While understanding these parameters is critical from the standpoint of signal measurement, stable allocation of bioprobes on CNTs using suitable coupling chemistries is a requirement for selective and sensitive recognition of target analytes. Several surface chemistries have been studied in great detail involving the use of side-wall/end-tip functionalization of CNTs for bioconjugation purposes (Gao and Kyratzis, 2008). However, among all the different metals used for surface functionalization, gold is better-known for its superior biocompatibility and ability to allow for stable immobilization of biomolecules either via self-assembled monolayers (SAMs) or direct physisorption (Love et al., 2005) on its reactive surface. Recently, architectures combining gold and CNTs have garnered considerable attention as they allow for the integration of their individual unique properties to develop potentially more versatile systems. It has been shown that owing to its high conductivity, electro-deposition of gold on CNT tips also allow for better control of electrode current density (Yun et al., 2007, Yun et. al., 2008). These studies laid the framework for the present work to explore such CNT-gold based architectures and their functionalization to better detect specific biomarkers involving bone turnover.

Therefore, the objective of this study is to develop an electronic label-free carbon nanotube-based biosensor for c-terminal telopeptide detection using EIS. Extra-long vertically aligned CNT (VACNT) posts were utilized to prepare the conducting electrodes, and were further electrodeposited with gold nanoparticles on their tips. The vertical alignment of CNTs allowed for controlled exposure of the area utilized for electrode/biosensor testing, which in turns controls the electrode current density, thus enhancing reproducibility and precision. The addition of gold to the biosensing system eliminated the need for CNT functionalization for biosensing component attachment due to the biocompatibility and protein immobilization properties of gold. The CNT electrode preparation, gold deposition conditions and the chemistries used for bio-conjugation were accordingly optimized. The immobilization of cTx antibody on the gold modified CNT electrode enabled the development of cTx telopeptide biosensor. In order to demonstrate feasibility of the sensor developed for point-of-care (POC) applications, the frequency most sensitive to changes in the impedance following the antigen–antibody interaction was determined and then used for the detection of the various marker concentrations by measuring the changes in impedance at a single frequency. Furthermore, this single frequency testing of various concentrations of cTx in the presence of protein interference was also demonstrated as described in the current work.

2. Materials and methods

2.1. Materials

Non-conducting Epicure epoxy resin and silicon carbide papers of the desired grit size were purchased from Buehler (Lake Bluff, IL). Silver epoxy paste was purchased from AI Technology, Inc. (Princeton, NJ). Hydrogen tetrachloroaurate was purchased from Sigma Aldrich (St. Louis, MO). Phosphate buffer solution (10 mM PBS) was purchased from the Lonza Group Ltd. (Walkersville, MD). Potassium ferrocyanide trihydrate and potassium ferricyanide was purchased respectively, from Fisher Scientific, Inc. (Fair Lawn, NJ). Neutravidin and bovine serum albumin (BSA) was purchased from Thermo Fisher Scientific (Rockford, IL). Biotinylated C-terminal telopeptide antibody and the human C-terminal telopeptide antigen were obtained from Serum CrossLaps ELISA Kit were purchased from Immunodiagnostic Systems (Scottsdale, AZ). Dulbecco's Eagle Medium containing (DMEM) 4.5 g/L glucose, L-glutamine, and sodium pyruvate was purchased from Cellgro (Corning Life Sciences, Manassas, VA). Millipore Deionized (DI) water with a resistivity of 18.2 MΩ cm was used for all rinsing purposes.

2.2. Fabrication of gold deposited VACNT electrodes

Vertically aligned carbon nanotube posts (VACNTs) were grown on Si-wafers using thermal chemical vapor deposition (CVD) process as described in the earlier reports (Chakrabarti et al., 2007; Landis et al., 2010; Yun et al., 2006). The annealed posts were peeled individually from the silicon wafer, mounted in non-conducting epoxy, and degassed for at least 30 min to remove any bubbles. The individually mounted VACNT posts were then allowed to cure under room temperature conditions for approximately 8 h. Following this, the epoxy mounted posts were polished on one end to 50 μm using silicon carbide polishing paper. Electrical contact of the exposed nanotubes with copper wire was made using a silver epoxy paste. Non-conducting epoxy was again employed to insulate the region of contact between VACNTs and copper wire following which; it was cured for approximately 8 h under room temperature conditions. The epoxy was then polished to 50 nm to expose the other end of the VACNTs. The electrodes were cleaned ultrasonically thrice in absolute ethanol and DI water for 2 min each, in between the polishing steps. The electrodes were then subsequently rinsed in DI water and dried. Gold was electrodeposited using 0.08 M hydrogen tetrachloroaurate

solution by applying a potential of 0.175 V vs. Ag/AgCl. The gold coated electrodes were finally rinsed in DI water and allowed to dry under room temperature conditions.

2.3. Biosensor preparation and testing

The gold coated VACNT electrodes were treated with 1 mg/mL neutravidin prepared in 10 mM PBS, pH 7.4 for 12 h at 4 °C. The avidinated electrodes were then immobilized with 0.8 μg/mL of biotinylated cTx antibody prepared in 10 mM PBS for 8 h at 4 °C. This antibody is specific in its interaction with cTx. 1% bovine serum albumin (BSA) prepared in 10 mM PBS, pH 7.4 was used to block the unbound sites on the electrode. The electrodes were then placed in PBS buffer (control solution) and were ready for testing. Various concentrations of cTx were prepared ranging from 0.05 ng/mL to 0.6 ng/mL, thus targeting a lower range of cTx to improve the lower limit of detection. The developed sensor was then treated with antigen for 1 h following which, the electrode was rinsed in DI water and impedance measurements were then made. For evaluating the protein interference, various concentrations of C-terminal telopeptide were also prepared in DMEM with 10% fetal bovine serum (FBS) incorporated following which impedance measurements were made as above. Resulting Nyquist plots were analyzed using Z-view (Scribner Associates, Inc.) to determine the charge-transfer resistance values, and single-frequency plots were analyzed using the Gamry EChem Analyst (Gamry Instruments, Inc.).

2.4. Microscopy and electrochemical characterization

Raman miroscopy (Renishaw in Via Raman Microscope 633 nm red laser) and scanning electron microcopy (SEM, Philips XL30, operating voltage: 10–20 KV) was used to characterize the obtained VACNTs/Au-VACNT electrodes. Electrochemical characterization was carried out using the Gamry series G Potentiostat (Gamry Instruments, Inc., Warminster, PA). ZView software (Scribner Associates) was used for modeling of the impedance data. Cyclic voltammetry was conducted in 1 M KNO_3 containing 6 mM $K_3[Fe(CN)_6]^{3-}$ electrolyte solution across a potential range of −0.2 V to 0.8 V at various scan rates, and electrochemical impedance spectroscopy (EIS) characterization was executed in an electrolyte solution consisting of 5 mM of potassium ferrocyanide/ferricyanide redox couple in 10 mM PBS. All the EIS experiments were carried out across a frequency range of 300,000–0.01 Hz with an AC voltage amplitude of 10 mV rms and were repeated until the response was stable. Platinum wire was used as the counter electrode and Ag/AgCl was used as the reference electrode.

3. Results and discussion

3.1. VACNT characterization

The material scaffold used for biomolecular immobilization plays a critical role in terms of the final sensor characteristics. In the case of carbon nanotubes, the nanotube length and bundle diameter significantly affect the electrode charge transfer reaction rates, background noise and reproducibility of the electrochemical sensor. Therefore, the VACNTs grown using the CVD process were first characterized using Scanning Electron Microscopy (SEM) and Raman Microscopy. Fig. 1A–C shows the SEM images of the

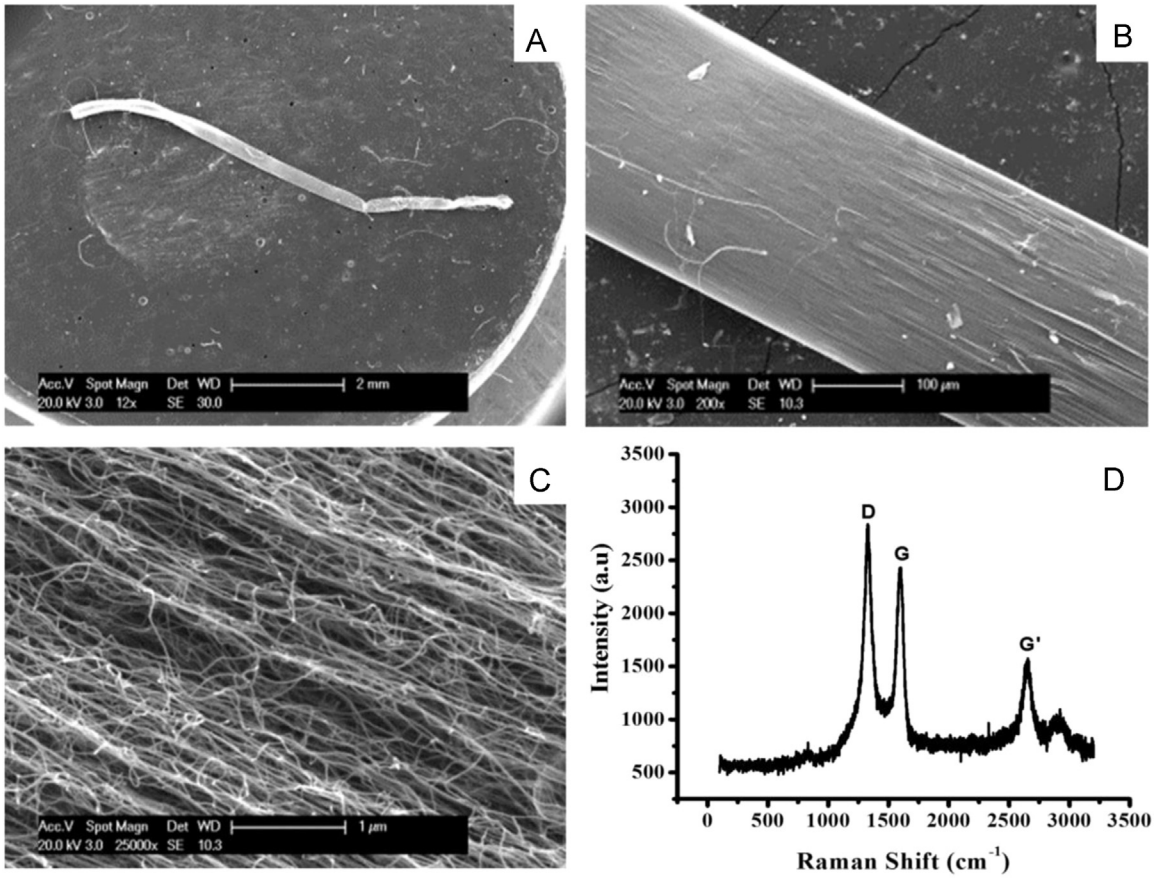

Fig. 1. SEM images of VACNT posts at (A) 12 × magnification, (B) 200 × magnification, and (C) 25,000 × magnification; (D) Raman spectrum of VACNT posts with D (defect/disorder band), G (graphene/order band), and G′ (graphite band) indicated above respective peaks.

VACNTs at various magnifications. From Fig. 1A and B, the approximate tube length of the nanotubes was estimated to be ~8 mm and the bundle diameter was determined to be ~200 μm. Fig. 1D shows the Raman spectrum of the VACNT posts (unpublished results previously presented at the 2011 Electrochemical Society Meeting). The G′ peak at approximately 2640 cm^{-1} represents the long range order, the interaction between the graphene layers in the multi-walled carbon nanotubes. The D and G bands at 1330 cm^{-1} and 1580 cm^{-1} correspond to the disordered and ordered carbon bands in carbon nanotubes respectively. The ratio of the intensity of the D and G bands is indicative of the quality and purity of the CNTs, with lower ratios indicative of CNTs with higher purity and lesser defects. It was found that the CVD-grown VACNT posts had an I_D/I_G ratio of ~1.1, indicating that the VACNTs utilized in this study had a higher degree of disorder and impurities in their as-grown structure. Therefore, the CNTs utilized in this study had a higher degree of impurities, and the expression of these impurities in the electrochemical experimentation could have had a negative effect on the reproducibility and precision of the biosensing system.

3.2. VACNT and gold-coated VACNT electrode characterization

The electrochemical properties of the VACNTs were then evaluated with or without the electrodeposition of gold, the process schematic shown in Fig. 2. This was done by fabricating the CNT electrodes followed by electrodeposition with gold (see Fig. 2), and comparing those to CNT electrodes without gold electrodeposition (Fig. 3). Fig. 3A shows the cyclic voltammetry of plain and 5 s gold electrodeposited CNT electrode in 1 M KNO_3 containing 6 mM $K_3[Fe(CN)_6]^{3-}$. In the case of plain CNT electrodes, despite the presence of a higher degree of disorder determined in the nanotube structure as observed with the Raman studies discussed above, the presence of peak currents with a ratio equaling one indicates the reversibility of the iron redox couple for the corresponding oxidation and reduction reactions occurring on the CNT electrodes, thus validating the Nernstian behavior of the plain CNT electrodes. Therefore, despite the higher degree of disorder and impurity, all the electrodes display Nernstian behavior, implying that all the electrodes had similar electron-transfer and gold electrodeposition characteristics and would therefore behave in a similar manner upon functionalization. The peak separation voltage for the redox probe was observed to be approximately, 100 mV for the plain uncoated CNT post electrode. Furthermore, the effective area of the electrode was calculated using the Randle–Sevcik equation given below.

$$i_p = 2.69 \times 10^5 n^{3/2} D^{1/5} C_0 v^{1/2} A_{eff} \quad (1)$$

where i_p is the peak current, n is the number of electrons transferred in the redox reaction, D is the diffusion coefficient (7.6×10^{-4} cm^2/s), C_0 is the concentration of the redox couple (6 mM), υ is the scan rate (100 mV/s), and A_{eff} is the effective surface area of the electrode. It was determined that the plain CNT electrodes had an effective surface area of 4.4×10^{-4} cm^2.

Electrodeposition of gold on the CNTs increased the peak currents and consequently, the effective surface area calculated from the Randle–Sevcik equation increased to 5.3×10^{-4} cm^2. Additionally, the gold coating decreased the peak separation voltage indicating that gold improved the electron transfer kinetics of the system. The peak current ratio was approximately 1.0 for gold deposited electrodes, validating the Nernstian behavior of the electrodes. Fig. 3B demonstrates the square root of scan rate relationship on the peak currents of plain and gold deposited CNT electrodes, further validating the reversible electron transfer

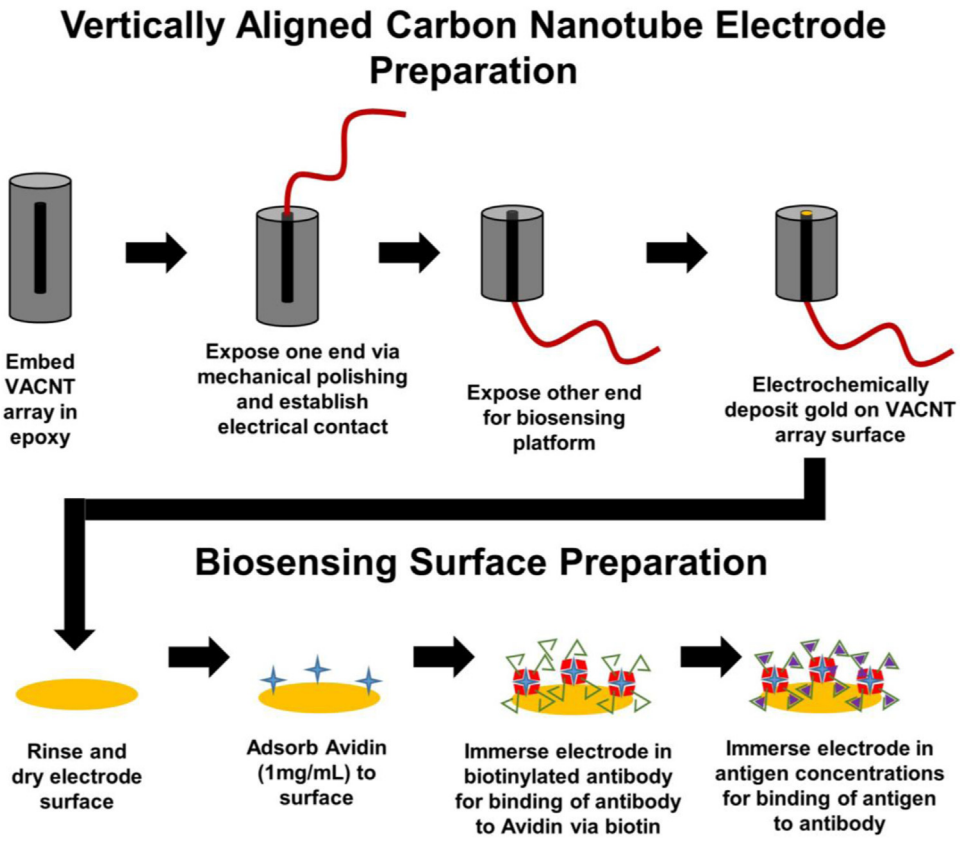

Fig. 2. Schematic demonstrating the fabrication of the vertically aligned carbon nanotube (VACNT) electrodes, the time of gold electrodeposition, and the various steps required to prepare the biosensing surface on the electrodeposited gold.

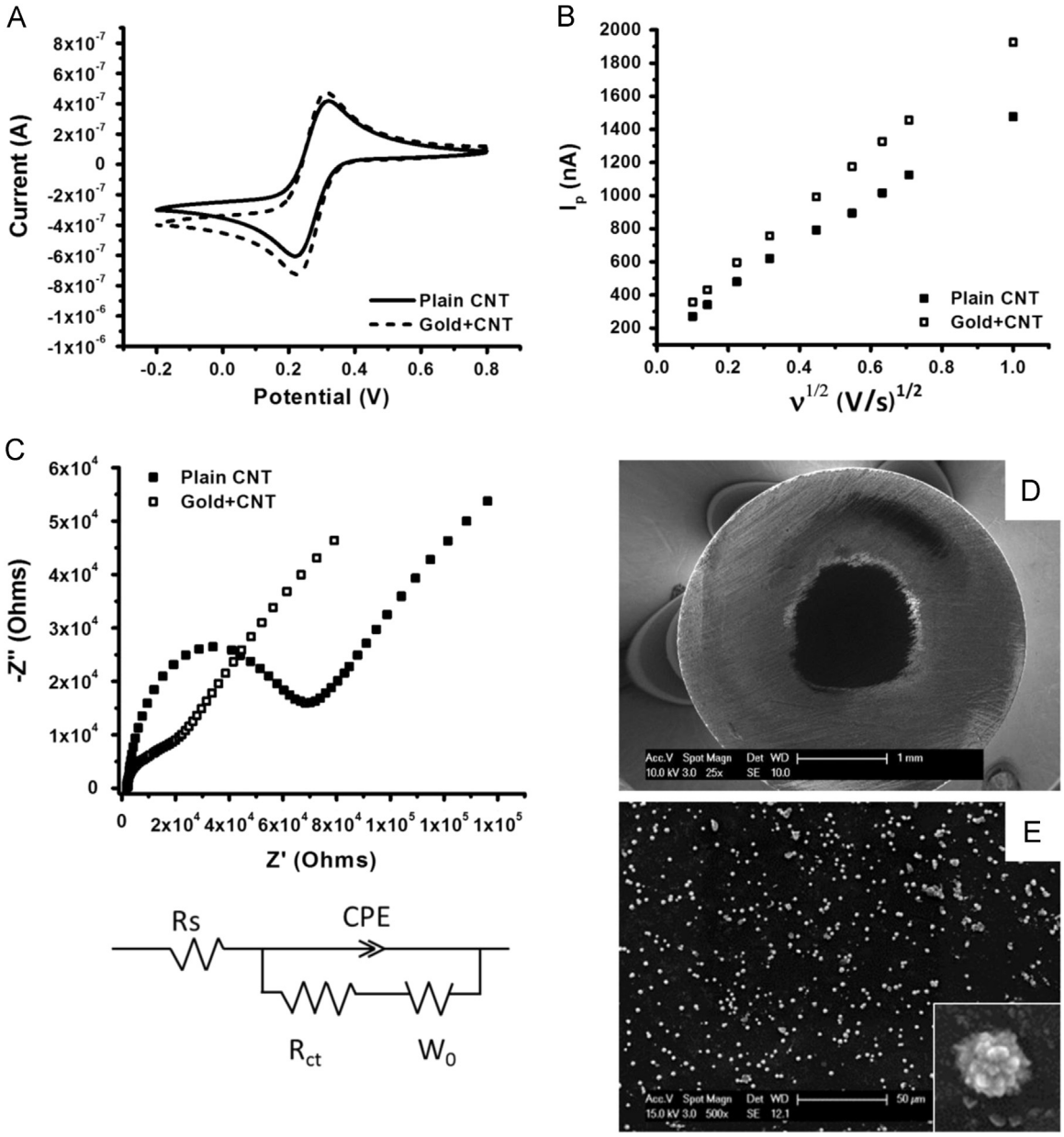

Fig. 3. Characterization of VACNT posts electrodes before and after gold deposition characterized (A) cyclic voltammetry (CV) for plain VACNT electrode and 5 s gold electrodeposited VACNT electrode conducted in 1 M KNO_3 containing 6 mM $K_3[Fe(CN)_6]^{3-}$ (B) the influence of square root of scan rate on peak current for plain and 5 s gold electrodeposited VACNT electrodes (C) Nyquist depiction of electrochemical impedance spectroscopy (EIS) for plain and 5 s gold electrodeposited VACNT electrodes conducted in 10 mM PBS, pH~7.4 containing 5 mM $[Fe(CN_6)]^{3-/4-}$ for an amplitude of 10 mV over a frequency range of 0.1 Hz–300 KHz at open circuit potential with corresponding equivalent circuit shown below (D) SEM of plain VACNT electrode at 25 × magnification (E) SEM of 5 s gold electrodeposited on CNT electrodes at 500x magnification with an inset of and SEM of a single cluster of gold nanoparticles at 50,000 × magnification.

kinetics of the system. The nearly 1.0 ratio of peak currents and the linear relationship of the square root of scan rate to the peak currents were indicative of the reversible nature of the electrodes both with and without the deposition of gold, thus establishing that the system is at equilibrium and that electron transfer-kinetics are fast enough to maintain the surface concentrations throughout the redox process. The increased peak currents and the decreased peak separation with the deposition of gold was indicative of a more improved reversible system due to the better expected conductivity and electron-transfer kinetics. Fig. 3C shows the Nyquist plots obtained by impedimetric characterization of the plain CNT and Au-CNT electrode. Under the Nyquist plot is the corresponding equivalent circuit that was used to model the impedance response experimentally obtained to best represent the physical structure of the interface. The observed semicircular region of the plot associated with electron transfer processes is represented by a parallel circuit representation of a resistor (R_{ct}) and the constant phase element (CPE). The tail at the lower frequencies indicates the presence of diffusion limited electrochemical processes, which is represented using the Warburg element (W_o). The solution resistance is represented by R_s. As observed in the Nyquist plots, the charge transfer resistance (R_{ct}) that characterizes the interfacial electron transfer resulting from the Fe^{2+}/Fe^{3+} redox couple, decreases with gold deposition. This observation is concurrent with an increase in the linear portion of the spectrum indicating the dominance of the diffusion-limited electrochemical processes and hence, faster electron transfer processes, which is consistent with the increasing peak current values for the Au deposited CNT (Au-CNT) electrodes observed in the cyclic voltammograms (CV) in Fig. 3A.

SEM was performed to characterize the surface morphology of the gold electrodeposited on the CNT electrodes. Fig. 3D shows the SEM image of a non-gold-coated VACNT embedded in the epoxy resin at low magnification. Fig. 3E shows the SEM image taken on the gold-coated VACNT electrode, with each set of particles indicating one carbon nanotube in the VACNT array. The electrodeposited gold nanoparticles were spherical and their size was found to be in the range of 2–3 μm with an average distribution density of 40 particles/VACNT in the array, with the inset image demonstrating the morphology of the gold nanoparticles taken at 10,000× magnification. Accordingly, the estimated area of the gold-coated VACNT electrode was $\sim 5.1 \times 10^{-5}$ cm^2. The lower values of the area obtained from the SEM image in comparison to the effective electrode area determined from the Randle–Sevcik equation may be due to the fact that the current from a CV is representative of the entire three dimensional electrode, while the image used for area calculations from SEM takes into account only the two dimensional nature of gold nanoparticles deposited on the CNT electrode. Thus, the studies from CV, EIS, and SEM show that despite the high disorder to order ratio of the carbon nanotubes, the CNT electrodes fabricated show reversible electrochemical kinetics for redox couple used in the current study and enable electrochemical deposition of gold nanoparticles. The electrochemical similarities could therefore allow for better precision and reproducibility of the biosensing system despite the disorder and impurities present at the CNT fabrication stage. It should be noted that while the primary aim of depositing gold nanoparticles was to enhance the ease of immobilization of the biosensing elements, the CV and EIS studies show that gold nanoparticles also enhance the electrochemical properties of the CNT electrode. In addition, the inert nature of gold will reduce the toxicity of the biosensor to biomolecular environments.

3.3. Biosensor immobilization layer characterization

Electrochemical impedance spectroscopy (EIS), where a redox probe added to the analyte solution transduces the antigen–antibody interactions at the electrode interface into a measureable electrical signal for detection, is usually very sensitive, especially when changes in the real component (charge transfer resistance, R_{ct}) of the impedance spectrum measured. This is due to the fact that these changes are much higher than the changes in capacitance arising from the imaginary component of impedance. The gold-coated VACNT electrode was characterized through EIS at every stage of preparation of the sensor. Fig. 2 outlines the schematic of the processes used for biomolecular immobilization on the gold-coated VACNT electrode, and Fig. 4 shows the corresponding impedance spectra obtained on the gold-coated VACNT electrode following the immobilization of avidin and biotinylated antibody. As with the gold-coated VACNT electrode, there is an observed semicircular region of the plot associated with the electron transfer processes, represented by the parallel circuit combination of a resistor in parallel with the constant phase element (CPE) shown in the equivalent circuit in Fig. 3C. At lower frequencies, the presence of diffusion limited electrochemical processes is represented using the Warburg element as outlined earlier. The Nyquist plots showed a higher charge transfer resistance for the electrodes immobilized with avidin and biotinylated antibody when compared to the plain gold-coated VACNT. This increase in charge transfer resistance arises from the insulating interfacial protein layers immobilized on gold expectedly serving as a barrier for the charge transfer of the ferro/ferricyanide redox probe. Further, it was noted that the equivalent circuit used to fit the experimental results following the immobilization step continued to be best represented by a constant phase element with a parallel resistor and Warburg impedance similar to the inset shown in Fig. 3C, thus indicating that the physical structure of the electrode interfacial layer was similar to that of the electrode prior to avidin immobilization. Following the immobilization of the antibody, the developed sensor was blocked with 1% BSA to prevent non-specific interactions. The introduction of BSA to the system resulted in a further increase in impedance of the biosensing system, thus indicating that BSA is indeed bound to the system and had presumably blocked any exposed surfaces or binding sites that were not occupied, thus ensuring that the future changes in impedance would only be the result of antigen binding to the antibody. The biosensors were then stored in 10 mM PBS at 4 °C until biosensor response testing.

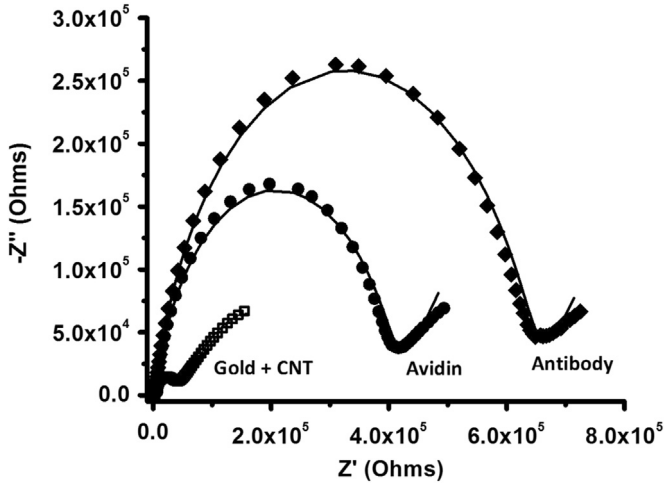

Fig. 4. EIS characterization depicted as Nyquist plots demonstrating the increase in charge transfer resistance upon avidin (1 mg/mL in PBS) and biotinylated C-terminal telopeptide antibody (0.8 μg/mL in PBS) immobilization on gold-coated VACNT electrodes conducted in 10 mM PBS, pH ~ 7.4 containing 5 mM $[Fe(CN_6)]^{3-/4-}$ for an amplitude of 10 mV over a frequency range of 0.1 Hz–300 KHz at open circuit potential.

3.4. Charge-transfer resistance-based biosensor response

Upon removal from storage, the biosensor was tested using the control solution, 10 mM PBS, thus establishing a baseline value (0.00 ng/mL). Testing proceeded with incubating the biosensor with known concentrations of c-terminal telopeptide for 1 h. The sensor was then rinsed in DI water and the impedance was measured at open circuit potential employing a 10 mV amplitude over a frequency range of 0.1 Hz–300 KHz.

Fig. 5A presents the impedance spectra obtained on the sensor exposed to various concentrations of cTx. A progressive increase in the semicircle diameter with increasing concentrations of cTx can be observed, thus demonstrating an increase in the charge transfer resistance due to the antigen–antibody interaction expected to occur at the electrode interface. The calibration curves were then generated with the R_{ct} parameter obtained from the theoretical fits, and the percent change in response was calculated using the formula below.

$$\%\text{Change in } R_{ct}\left(\frac{\Delta R_{ct}}{R_{ct0}}\right) = \frac{R_{ct\ sample} - R_{ct0}}{R_{ct0}} \times 100$$

Fig. 5B shows the calibration curve wherein the percent change in R_{ct} is plotted for 0.05 ng/mL, 0.1 ng/mL, 0.2 ng/mL, 0.3 ng/mL, 0.4 ng/mL, 0.5 ng/mL and 0.6 ng/mL of cTx. The developed impedimetric sensor responds linearly to the tested cTx concentrations with a correlation coefficient of 0.98, and the charge transfer resistance values fall within the 2.0×10^6–5.0×10^6 Ω range, which is similar to the charge transfer resistance range for those concentration levels reported earlier (Yun et al., 2007). The error bars

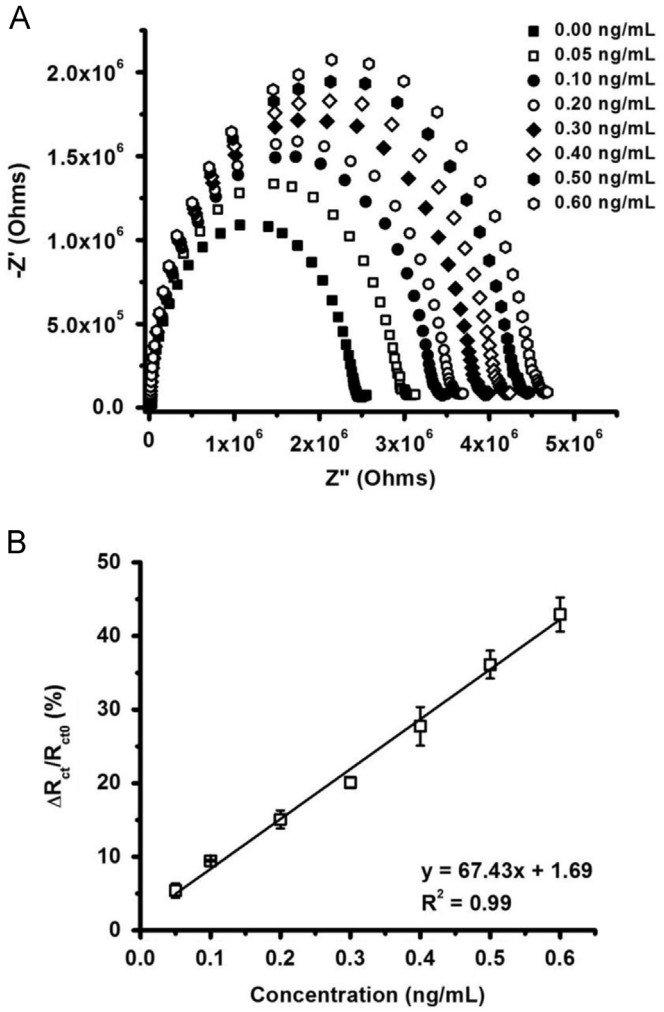

Fig. 5. (A) EIS characterization depicted as Nyquist interpretations demonstrating the increase in charge-transfer resistance with increasing concentrations of C-terminal telopeptide, conducted in 10 mM PBS, pH~7.4 containing 5 mM $[Fe(CN_6)]^{3-/4-}$ for an amplitude of 10 mV over a frequency range of 0.1 Hz–300 KHz at open circuit potential, and (B) EIS-corresponding calibration curve showing percent change in charge transfer resistance to different concentrations of C terminal telopeptide (error bars based upon standard error for $n=3$).

indicate the standard error for $n=3$, demonstrating error range for the three electrodes that were subjected to all concentrations, starting with the lowest concentration with gradual increase in concentration. Concentrations as low as 0.05 ng/mL produced a measureable signal, thus indicating the ability of the biosensor to detect extremely low concentrations of cTx. This is a significant improvement over previously reported detection limit of 50 ng/mL (Yun et al., 2007) wherein, gold was micropatterned on a silicon wafer and functionalized with cTx antibody. The detection limits obtained using standard analytical techniques such as an ELISA assay is in the range of ~0.02 ng/mL (Serum CrossLaps CTx-1 ELISA Kit, ImmunodiagnosticSystems), which is indeed lower than the value obtained from the current biosensor (0.05 ng/mL) although not diminishing the promise of the current impedimetric sensor approach. Therefore, further experimentation and refinement of this system would be required to achieve a lower limit of detection without sacrificing reproducibility or precision, as the current system has larger error margins than desired. The ideal limit of detection for the biosensing system would be ~0.01 ng/mL or lower to prove its superiority over the ELISA and to demonstrate extremely minute and accurate measurements. However, at this preliminary stage, it should be noted that the impedimetric sensing technique discussed in this manuscript represents a more rapid, much simpler, and potentially more cost-effective biochemical marker detection method upon further refinement and miniaturization of the system.

3.5. Single-frequency resistance-based biosensor response (with and without protein interference)

As mentioned earlier, the developed biosensor in this study has greater potential to be used for point-of-care (POC) applications for prognostic purposes if the tested frequency range were narrowed down to a single frequency making it even more simple and at the same time effective. One of the major advantages of implementing the single frequency testing is that in addition to simplifying the data analysis that would not require modeling to extract the relevant electrochemical parameters, it would significantly reduce the time required for actual testing of the impedimetric sensor response. The lower frequency range is relatively more sensitive to quantify the antigen–antibody binding parameter as given by the charge transfer resistance. However, as in the case of Faradiac impedance spectroscopy, higher impedance and signal drift result in higher noise at very low frequencies. In the demonstrated biosensing system, there are no highly pronounced differences in impedance at higher frequencies with increasing concentrations; however more pronounced differences in impedance were visible at frequencies lower than $f=200$ Hz (Fig. 6A), and the frequencies with the highest changes in impedance with increasing concentration were determined to be less than $f=50$ Hz (Fig. 6B). Thus, based on the analysis of the Bode plots (Fig. 6A and B) corresponding to the Nyquist plots, the frequency of $f=18.75$ Hz was determined to have optimal signal to noise ratios producing not only a detectable but also reproducible response for the developed sensor. Frequency determination was assessed by examining the linearity and correlation of percent change in impedance vs. concentration for each frequency and assessing the highest frequency with the best correlation and highest percent change in impedance at each percent increase in concentration. It should be noted that the Nyquist plots, unlike Bode plots, are not a function of frequency, making it impossible to determine which point on the Nyquist plot represents the chosen frequency. Single-frequency experiments at $f=18.75$ Hz were conducted for approximately 30 s per concentration (electrodes were incubated with concentrations for 1 h/concentration), which was the approximate time necessary for the resulting impedance to stabilize sufficiently.

Fig. 6C shows the calibration curve where the percent change in absolute impedance (Z_{mod}) is plotted for concentrations of cTx ranging for 0.05 ng/mL–0.6 ng/mL. The single-frequency impedimetric biosensor responds linearly to the increasing cTx concentrations with a correlation coefficient of 0.96 ($n=3$), thereby showing the potential of the developed system for translation into a possible portable sensor for point-of-care (POC) applications. In addition, the slope of the linear fit increased more than four-fold from 67.43 ΔR_{ct}/ng/mL (charge-transfer resistance based) to 302.83 ΔZ_{mod}/ng/mL (single-frequency resistance based). This increase is the result of only measuring at one frequency rather than taking multiple frequencies into account, thus reducing the amount of variance and increasing the sensitivity of the biosensor – a higher slope is indicative of enhanced sensitivity, allowing for smaller changes in concentration to be represented as larger percent change values. The single-frequency based method could detect concentrations as low as 0.05 ng/mL, just like the charge-transfer resistance-based method. Additionally, it should be noted that the single-frequency impedimetric biosensor demonstrates a linear response with a credible correlation coefficient of 0.91

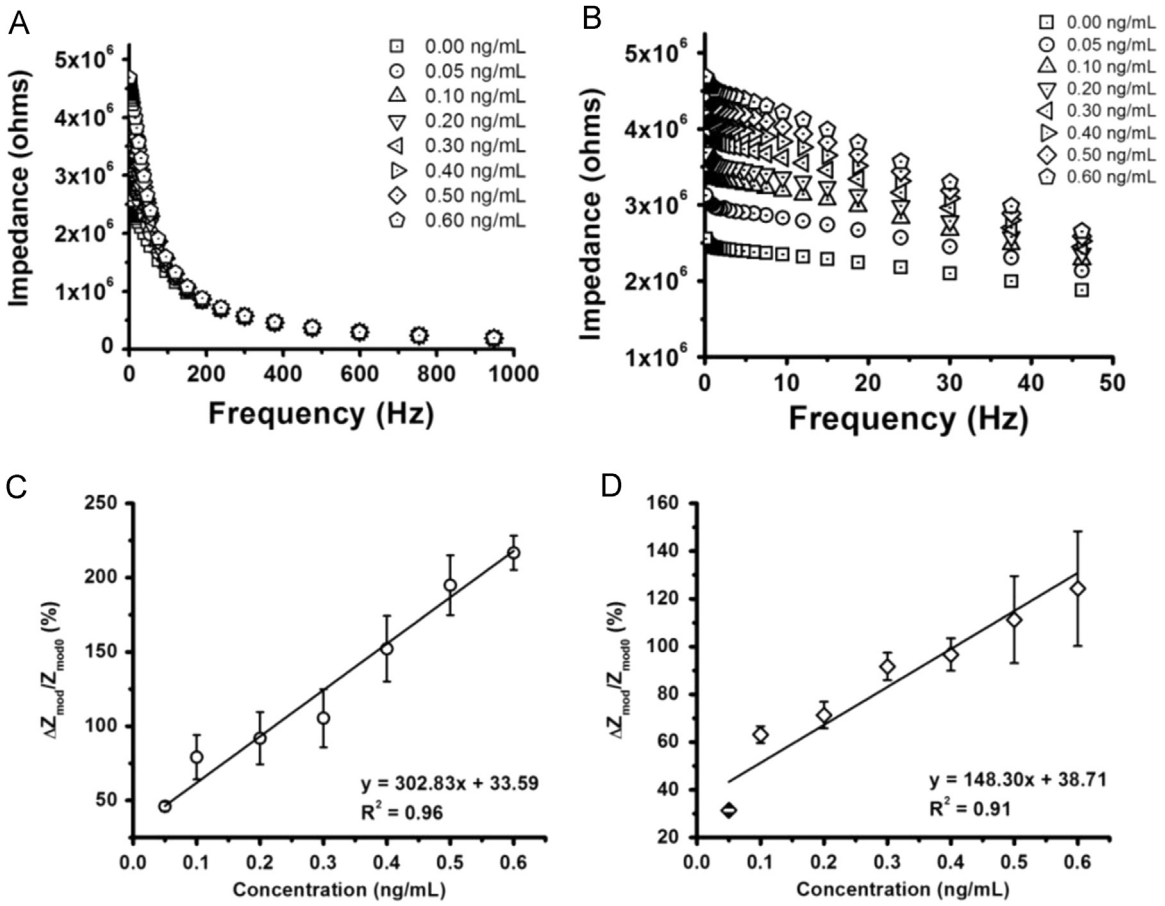

Fig. 6. (A) Bode plot showing impedance at frequencies (0.1–1000 Hz) for each increasing concentration of c-terminal telopeptide (B) Bode plot focused on frequencies 0.1–50 Hz for increasing concentration of c-terminal telopeptide (C) Calibration curve showing percent change in absolute impedance with increasing concentrations of C-terminal telopeptide when tested at 18.75 Hz (Error bars based upon standard error for $n=3$), and (D) Calibration curve showing percent change in absolute impedance at 18.75 Hz with increasing concentrations of C-terminal telopeptide prepared in DMEM solution in the presence of 10% fetal serum albumin (error bars based upon standard error for $n=3$).

($n=3$) to the increase in C-terminal telopeptide concentrations when in the face of interference from Dulbecco's Eagle Medium (DMEM) solution infused with 10% Fetal Bovine Serum (FBS) (Fig. 6D), thus demonstrating additionally, the ability of the impedimetric biosensor to successfully measure concentrations of cTx despite the protein/buffer interference, particularly at the lower concentration range (0.05–0.4 ng/mL), thus giving the gold-coated VACNT biosensor the added attribute of lower range detection. Once again, the limit of detection of the single-frequency electrodes, even with protein interference, was 0.05 ng/mL. However, the protein interference causes a decrease in the sensitivity of the biosensor, lowering the slope of the linear fit from 302.83 ΔZ_{mod}/ng/mL to 148.30 ΔZ_{mod}/ng/mL. This was due to the presence of additional salts and proteins present in the DMEM solution in comparison to the PBS solution. The additional salts and proteins can travel closely to the biosensing layer in the solution, and possible electrostatic interactions between the salts and proteins in solution could impact the biosensing surface and prevent the antigen from effectively binding. The most likely case is that the electrostatic interactions can draw the salts and proteins close to the biosensing layer, thus masking the binding sites on the antibody and preventing the antigen from binding, in turn reducing the sensitivity and correlation. In spite of this reduction in sensitivity in the face of interference, the biosensing system maintained a fairly high correlation coefficient ($R^2=0.91$), and the single-frequency based biosensor was still more sensitive than the charge-transfer resistance-based biosensor. These results therefore validate the use of the system in dynamic real time applications in practical environments using blood or other bodily fluids undeterred from the likely interference of multiple serums, enzymes, and proteins present in these fluids, especially due to the high specificity of the antibody. It should be also noted that there will be a wider variety of salts and proteins present in the blood than mimicked in the DMEM solution, so the use of a real whole blood sample may further decrease the sensitivity. Further testing and calibration would be further required to assess just how sensitive this system would be for detecting c-terminal telopeptide in whole blood. However, these results not only demonstrate reproducibility among biosensors ($n=3$), but also demonstrate the potential use of the gold-coated VACNT biosensors for not only bone biomarker but also other biomarker detection (provided the biomarker has a corresponding biotinylated antibody). With further refinement, calibration, and testing, both with prepared samples and whole blood samples, this system we believe has the potential to become an effective potential point of care (POC) diagnostic tool for monitoring the overall patient health condition. Therefore, these results presented serve as preliminary proof that such a system could be indeed developed with further experimentation.

4. Conclusions

In this study, we have demonstrated the development of an impedimetric biosensor for the detection of bone marker (cTx),

using VACNT electrodes as a template for gold electrodeposition to form a gold-coated VACNT electrode that can be functionalized with biosensing elements for biomarker detection. A linear trend was observed in the response curve plotted for the percent change in R_{ct} for tested concentrations with a lowest measurable signal of 0.05 ng/mL *c*Tx. Moreover, the feasibility of the developed gold-coated VACNT biosensor for point-of-care (POC) applications for diagnostic purposes was achieved by analyzing the absolute impedance values obtained above at single frequencies. It was determined that at 18.75 Hz, maximum and reproducible changes in impedance were observed for various concentrations with a trend in response which was again linear with good and credible correlation coefficient. Further ability to detect the bone marker in the presence of protein and buffer interference was also demonstrated using DMEM containing FBS, thus indicating the operation of the biosensor in a more biologically relevant fluid. The developed biosensor also allows for cTx concentration determination at very low levels. The results therefore demonstrate the potential efficacy of the impedimetric biosensor allowing for earlier indications of abnormalities in bone metabolism, while being also highly selective, with a low limit of detection, hence displaying great potential (with extensive additional experimentation, refinement, and miniaturization) for a simpler and more frequent assessments of bone metabolism monitoring at point-of-care thus likely improving patient care.

Acknowledgments

The authors acknowledge the partial financial assistance of NSF-ERC Grant # EEC-0812348 in supporting this work. The authors also acknowledge the financial support of the Swanson School of Engineering, University of Pittsburgh, while P.N.K. acknowledges the Edward R. Weidlein Chair Professorship, the Center for Complex Engineered Multifunctional Materials (CCEMM), and NSF-CBET Grant # 0933153 for support of use of equipment and accessories needed for this research.

References

Ahammad, A.J.S., Lee, J.J., Rahman, M.A., 2009. Sensors 9, 2289–2319.
Ajayan, P.M., 1999. Chem. Rev. 99, 1787–1800.
Burge, R., Dawson-Hughes, B., Solomon, D.H., Wong, J.B., King, A., Tosteson, A., 2007. J. Bone Mineral Res. 22, 465–475.
Burgeson, R.E., 1998. Annu. Rev. Cell Biol. 4, 552–577.
Chakrabarti, S., Kume, H., Pan, L., Nagasaka, T., Nakayama, Y., 2007. J. Phys. Chem. C 111, 1929–1934.
Daniels, J.S., Pourmand, N., 2007. Electroanalysis 19, 1239–1257.
Gao, Y., Kyratzis, I., 2008. Bioconjugate Chem. 19, 1945–1950.
Gong, K., Chakrabarti, S., Dai, L., 2008. Angew. Chem. 120, 5526–5530.
Katz, E., Willner, I., 2003. Electroanalysis 15, 913–947.
Landis, E.C., Klein, K.L., Liao, A., Pop, E., Hensley, D.K., Melechko, A.V., Hamers, R.J., 2010. Chem. Mater. 22, 2357–2366.
Love, J.C., Estroff, L.A., Kriebel, J.K., Nuzzo, R.G., Whitesides, G.M., 2005. Chem. Rev. 105, 1103–1170.
National Osteoporosis Foundation, 2012. Vol. 2012.
Okuno, S., Inaba, M., Kitatani, K., Ishimura, E., Yamakawa, T., Nishizawa, Y., 2005. Osteoporos. Int. 16, 501–509.
Rosenquist, C., Fledeliu, C., Christgau, S., Pedersen, B.J., Bonde, M., Qvist, P., Christiansen, C., 1998. Clin. Chem. 44, 2281–2289.
Ross, P.D., 1999. J. Clin. Dent. 2, 285–294.
Ryouji, M., Itsuo, Y., Masahiko, T., Yasuyo, H., Itsuaki, Y., Rikushi, M.J., 2000. J. Bone Miner. Metab. 18, 158–168.
Saito, N., Usui, Y., Aoki, K., Narita, N., Shimizu, M., Hara, K., Ogiwara, N., Nakamura, K., Ishigaki, N., Kato, H., Taruta, S., Endo, M., 2009. Chem. Soc. Rev. 38, 1897–1903.
Seeman, E., Delmas, P.D., 2006. N Engl. J. Med. 354, 2250–2261.
Siddiqui, S., Arumugam, P.U., Chen, H., Li, J., Meyyappan, M., 2010. ACS Nano 4, 955–961.
Srivastava, A.K., Macfarlane, G., Srivastava, V.P., Mohan, S., Baylink, D.J., 2001. Calcif. Tissue Int. 69, 327–336.
Tasis, D., Tagmatarchis, N., Bianco, A., Prato, M., 2006. Chem. Rev. 106, 1105–1136.
Yun, Y., Dong, Z., Shanov, V.N., Doepke, A., Heineman, W.R., Halsall, H.B., Bhattacharya, A., Wong, D.K.Y., Schulz, M.J., 2008. Sens. Actuators B: Chem. 133, 208–212.
Yun, Y., Dong, Z., Shanov, V.N., Schulz, M.J., 2007. Nanotechnology 18, 465505.
Yun, Y., Shanov, V., Schulz, M.J., Dong, Z., Jazieh, A., Heineman, W.R., Halsall, H.B., Wong, D.K.Y., Bange, A., Tu, Y., Subramaniam, S., 2006. Sens. Actuators B: Chem. 120, 298–304.